

# Optical Measurement of Forming Limit and Formability of Cu/Al Clad Metals

Tao Sun, Jin Liang, Xiang Guo, Maodong Ren, and Lizhong Wang

(Submitted June 18, 2014; in revised form January 28, 2015; published online February 20, 2015)

A digital image deformation measurement and analysis control system (XJTUDIC 8.0) was employed to measure the forming limit strain for Cu/Al clad metals produced via explosive welding technique. A contrast test between the digital image correlation (DIC) method and the conventional grid method was also implemented using the SPCC sheet metal forming limit test. The effect of heat treatment and contact status on forming limit was discussed based on the forming limit strain of Cu/Al clad metals. The interfacial and fracture structures were analyzed using scanning electron microscopy. The fracture site was predicted by finite element method. Results demonstrate that the forming limit curve of Cu/Al clad metals through DIC is more likely to reflect the formability of SPCC accurately. The forming limit of the clad with Al in the inner layer is higher than that of the clad with Cu in the inner layer. The formability of the annealed clads is superior to that of the non-annealed clads. The local interface failure induces the microcracks in Cu/Al clad metals during the forming process, which could be the main failure mode. With the finite element method, the fracture location of Cu/Al clad metals caused by uniaxial tensile during the forming limit test using DIC method is predicted accurately.

**Keywords** Cu/Al clad metals, digital image correlation, finite element method, formability, forming limit curve

## 1. Introduction

Clad metals are widely used in many aviation, shipbuilding, pressure vessel, and chemical applications because of their excellent integrated performance. However, the formability of clad metals varies with every material; hence, studies on the forming limit and failure mode of clad metals are practical and essential to changing traditional processing.

Several studies have been performed to estimate the formability of clad metals. Parsa (Ref 1) studied that the redrawing properties of aluminum stainless steel laminated sheet through simulations using finite element method (FEM). Liu et al. (Ref 2) deduced the forming limit strain expression of Cu-Al clad by adopting Hosford's high-order yield criteria and Marciniak and Kuczynski (M-K) theory, and they also developed a forming limit diagram through theoretical calculations. Tseng et al. (Ref 3) analyzed the fracture prediction of Al/Cu clad metals with different initial thickness ratios both numerically and experimentally. Sadighi (Ref 4) investigated the effect of blank holder forces on wrinkling and fractures in the drawing process of single and two layers. The measurement

method used to form the limit strain in the aforementioned work corresponds with the grid method with low level of accuracy and efficiency; this method provides beneficial information to the present study.

The traditional coordinate grid method partially satisfies the requirements of strain measurement but has the following shortcomings: (1) offline strain data acquisition strongly depends on the operator and thus results in low accuracy and efficiency; (2) the workload of grid drawing is large; and (3) this method can determine the final state of forming but cannot identify the instability of the sample.

Digital image correlation (DIC) is a full-field optical strain measurement method that is non-contact, highly accurate, has a minimal effect on the environment, and has a high degree of automatization. DIC method has been used to measure sheet forming limit strain because it overcomes the drawbacks of coordinate grid method. Vacher et al. (Ref 5) used 2D DIC to determine the forming limit curve (FLC) for 340 stainless steel alloys using a test similar to the Swift cup test. Hotz and Hanggi (Ref 6) demonstrated the use of 3D DIC for determining FLCs using the limiting dome height (LDH) test. In both cases, the final deformed images were directly compared with the initial un-deformed images without real-time visualization. Hijazi et al. (Ref 7) developed a modified LDH test tool with in situ 3D DIC to determine the FLCs for aluminum sheets. Pires et al. (Ref 8) measured deformations of aluminum A5052 alloy under thixocast condition using a digital camera coupled with a press. Palumbo et al. (Ref 9) used a DIC system to acquire strain maps during the AZ31 Mg alloy forming process in warm conditions while maintaining the equivalent strain rate constant. Using DIC, Zhang et al. (Ref 10) predicted the FLCs of sheet metals by combining tensile test with finite element M-K model. Palumbo et al. (Ref 11) embedded a DIC system (Aramis) in AZ31 formability equipment to determine the major and minor strains continuously and evaluate the moment and location of failures. Rohatgi et al. (Ref 12) developed and applied a novel experimental technique that combines

**Tao Sun**, State Key Laboratory for Manufacturing Systems Engineering, School of Mechanical Engineering, Xi'an Jiaotong University, Xi'an 710049 Shanxi, China and Department of Mechanical and Electrical Engineering, Sichuan Engineering Technical College, Deyang 618000 Sichuan, China; and **Jin Liang**, **Xiang Guo**, **Maodong Ren**, and **Lizhong Wang**, State Key Laboratory for Manufacturing Systems Engineering, School of Mechanical Engineering, Xi'an Jiaotong University, Xi'an 710049 Shanxi, China. Contact e-mail: sunmark2005@163.com.

high-speed imaging and DIC techniques to investigate the high-rate deformation behavior of aluminum sheets during electro-hydraulic forming. All of the experimental tests in these studies were implemented using a DIC system, which can acquire strain maps of the entire forming process. Most studies on forming limit tests generally analyze the FLCs of a single material during the forming process; only a few studies have focused on the deformation of clad metals based on DIC.

In the current research, a forming test setup with a DIC system was employed to measure the forming limit strain for Cu/Al clad metals. A contrast experiment of SPCC sheet metal forming limit between DIC and grid method was also conducted. Again, the effect on Cu/Al clad metal formability was discussed, and the fracture appearance of Cu/Al clad metal after forming test was probed by scanning electron microscopy

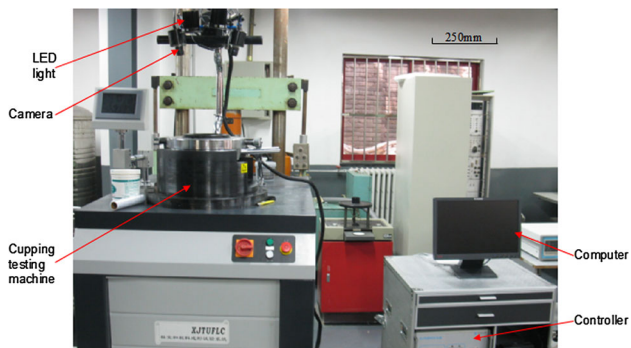


**Fig. 1** Forming test setup with the DIC system. (Color online only)

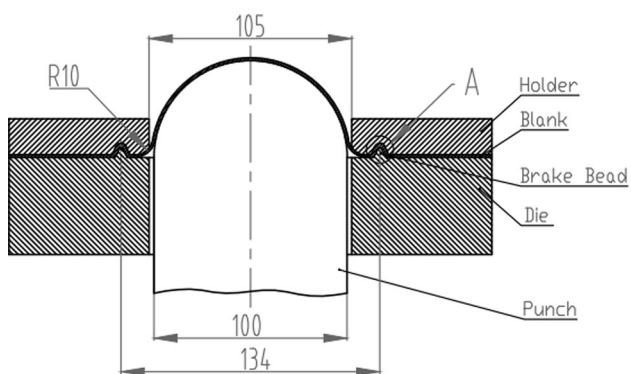


**Fig. 2** Software interface of the XJTUDIC 8.0 system: (1) project tree window for image list display, (2) OpenGL 3-D view for result display (3-D points/displacement/strain), (3) properties window for camera and speckle parameters display, (4) information browse window for project information display, (5) 2-D view for the left/right camera image display. (Color online only)

(SEM). Finally, a finite element model of Cu/Al clad metal was used to predict the fracture position.

## 2. Experimental Scheme

The forming test setup with a DIC system (Fig. 1) includes two industrial charge-coupled device cameras (with a resolution of  $1624 \times 1236$  pixels), two LED light sources, a computer, a controller (to control the LED light and computer), a cupping testing machine (BTP-60 with a stamping force of 0 to 300 KN), and a digital image deformation measurement and analysis control system (XJTUDIC 8.0, Fig. 2). The cameras were equipped with a 25-mm focal length lens (Schneider Kreuznach Xenoplan type) and fixed on the same horizontal plane at an angle of  $30^\circ$  to form a  $150 \text{ mm} \times 100 \text{ mm}$  field.

Copper (T2) and pure aluminum (1060) were employed to prepare the Cu/Al clad metal sheet specimens. The Cu/Al clad metal sheets were manufactured by Shen'ao Metal Material Corporation through explosion welding. The clad metal sheets were treated by annealing at  $280^\circ \text{C}$ ; unsintered sheets were also prepared. The mechanical properties of the clad metal sheets under different heat treatments were obtained by uniaxial tensile test (Table 1). The clad layer comprised 35% Cu and 65% Al, with a total thickness of 1 mm. The samples (Fig. 3) were cut with a wire electrical discharge machine (EDM) according to the ISO 12004-2: 2008 standard. A uniform coat of white spray paint was applied to the surface of each coupon followed by the application of black paint droplets to achieve a suitable grayscale contrast pattern required by the DIC algorithm.

The forming limit test was performed to evaluate the forming limit of the Cu/Al clad metal sheets; the experimental procedure is illustrated in Fig. 4. The clad metal sheets were clamped at their edges and stretched by a 100-mm diameter hemispherical punch as shown in Fig. 5. The stretch rate was set to 1 mm/s, with a camera framing rate of 10 frames/s. Specimens (180 mm long, with various widths from 30 to 180 mm) were prepared to cover various stretch modes. A PE film (with a thickness of 0.05 mm) covered with KLUBER grease was utilized for lubrication. The blank holding force was set to 150 kN. The relative proportions of the Cu and Al surfaces in contact with the punch were equal; the relative proportion was found to influence the formability of the Cu/Al clad metals. Square grids with a spacing of 35 pixels (4.4 mm/pixel) and a subset of  $33 \times 33$  pixels (4.4 mm/pixel) were utilized in the DIC postprocessing of the images. The detailed DIC data processing could be referred to in other literature (Ref 13, 14). Figure 6 shows the deformation conditions of the samples after reaching the forming limits. After the images underwent DIC postprocessing, the surface profile and strain

**Table 1** Mechanical properties of the Cu/Al clad metals under different heat treatments

	Young's modulus, $E/\text{GPa}$	Poisson's ratio, $\mu$	Yield strength, $\sigma_{0.2}/\text{MPa}$	Tensile strength, $\sigma_b/\text{MPa}$	Elongation $\delta/\%$	Strain hardening exponent, $n$	Strength coefficient, $K/\text{MPa}$
Not annealed	70.127	0.293	259.286	265.952	4.25	...	...
Annealed at $280^\circ \text{C}$	94.887	0.277	75.592	178.781	11.88	0.300	2658.958

In the uniaxial tensile test of non-annealed Cu/Al clad metals, the plastic deformation stage has not been observed, so strain hardening exponent and strength coefficient could not be obtained

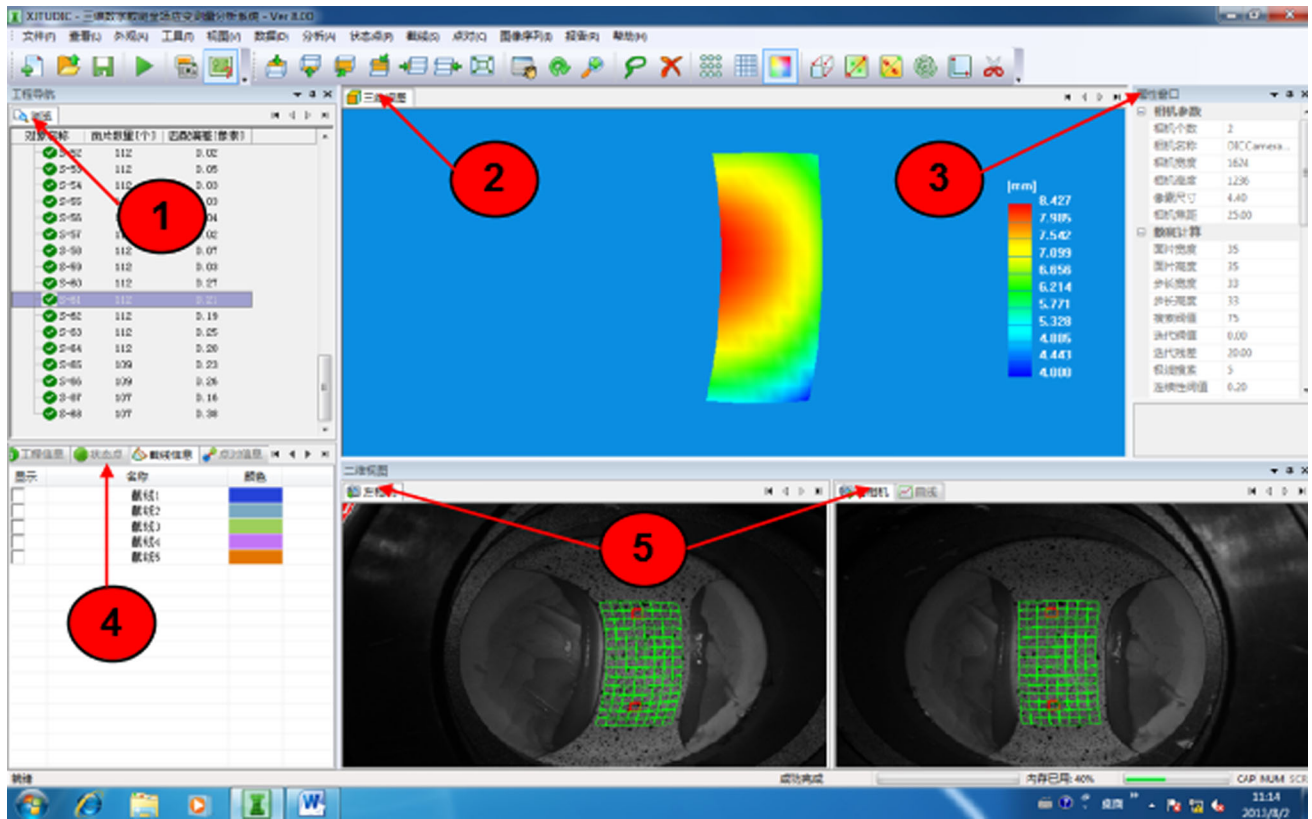


Fig. 3 Schematic of the samples' shape and dimension

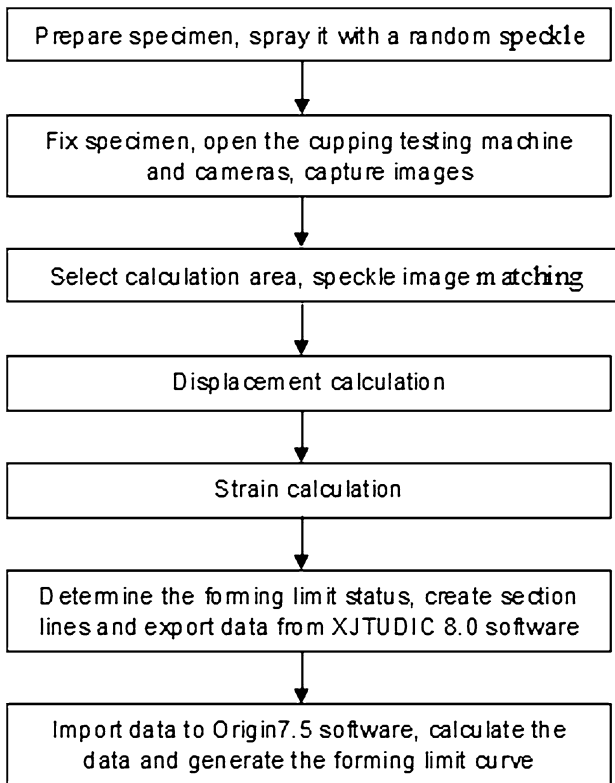


Fig. 4 Flow chart of the forming test

distribution of a sample under different deformation states were obtained (Fig. 7).

### 3. Experimental Results and Discussions

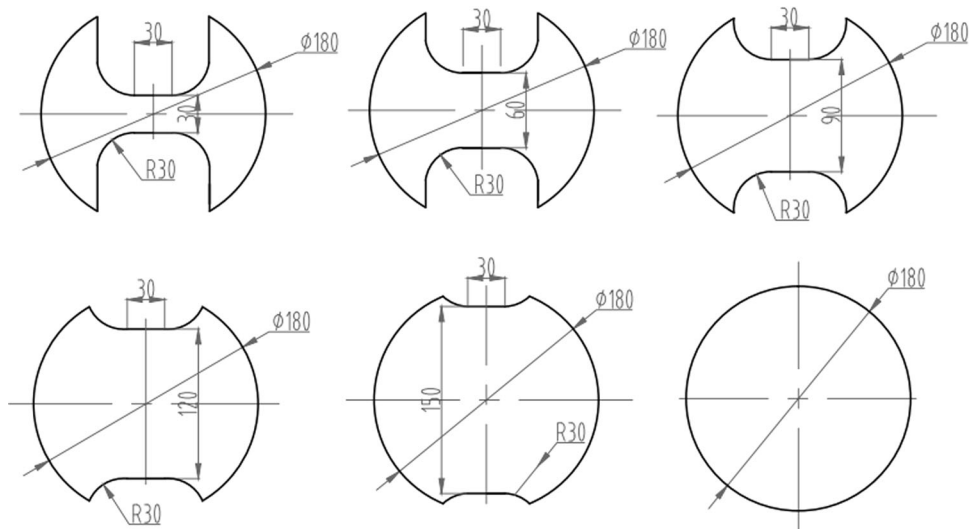
#### 3.1 Contrast Experiment of Limit Formation Between the DIC and Grid Methods

Using the experimental device in Fig. 1, a contrast experiment of SPCC sheet metal forming limit between DIC (The FLC of SPCC using DIC method can be seen in Fig. 8) and grid methods [XJTUSM system (Ref 15)] was conducted under the same test conditions. In both methods, the SPCC sheet metals belong to the same batch, and the samples have the same dimensions (Fig. 3). Figure 9 shows that two FLCs are obtained using the DIC and grid methods. The third FLC is calculated using the formula (Ref 16) provided by North American Deep Drawing Research Group (NADDRG). Figure 9 shows that the strain distribution of FLC obtained by the DIC method is close to the grid method, but the offline strain data of grid method are larger than the actual results. The FLC calculated using the formula by NADDRG is the highest. Thus, the forming limit of SPCC sheet metal might be overstated, and the results of the DIC method might be closer to actual results.

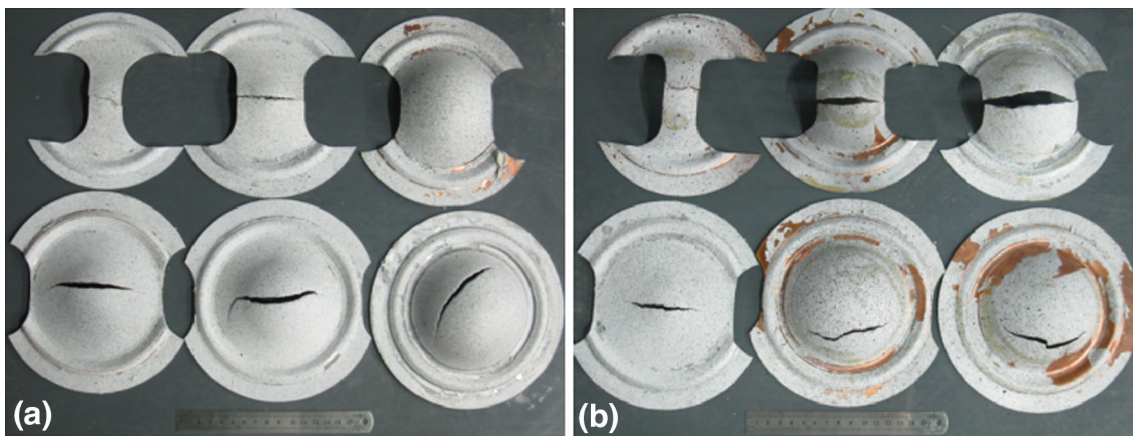
#### 3.2 FLC Results

Figure 10 shows that the FLCs of the Cu/Al clads with Al in the inner layer are higher than those of clads with Cu in the





**Fig. 5** Schematic of the testing machine's forming and blank holder part



**Fig. 6** Schematic of the samples' deformation conditions: (a) not annealed and (b) annealed at 280 °C. (Color online only)

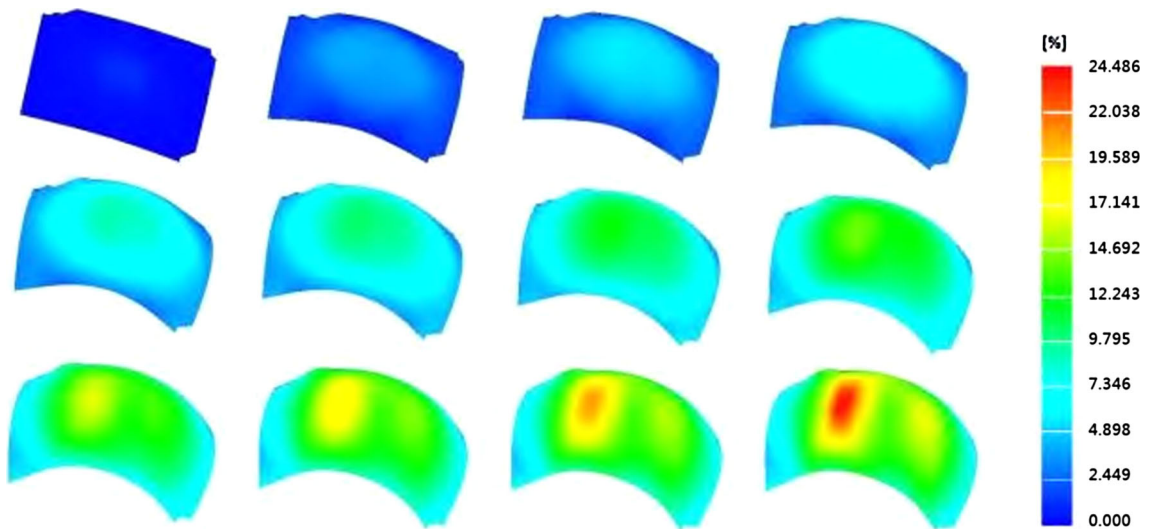


**Fig. 7** Surface profile and strain distribution of the samples under different deformation states when the width is 90 mm. (Color online only)

inner layer. Thus, the formability of clad metals with Al in the inner layer is superior to that of clad metals with Cu in the inner layer. This result might be because the strain hardening exponent ( $n$  value) of Cu is larger than Al under any circumstances. During the forming process, if the punch comes

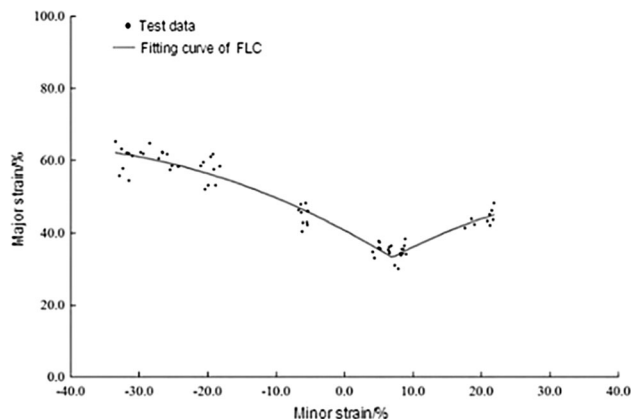


Fig. 8 The FLC of SPCC using DIC method

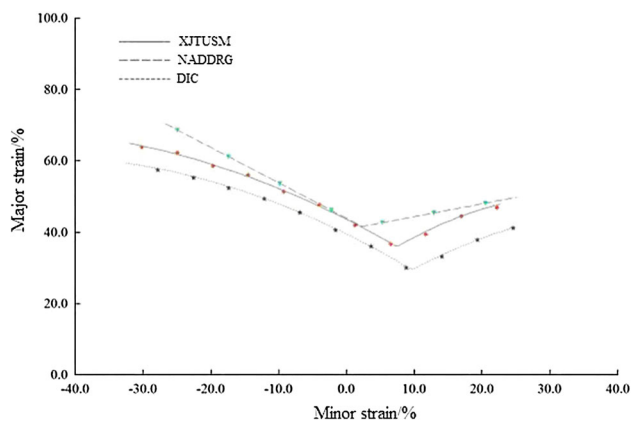
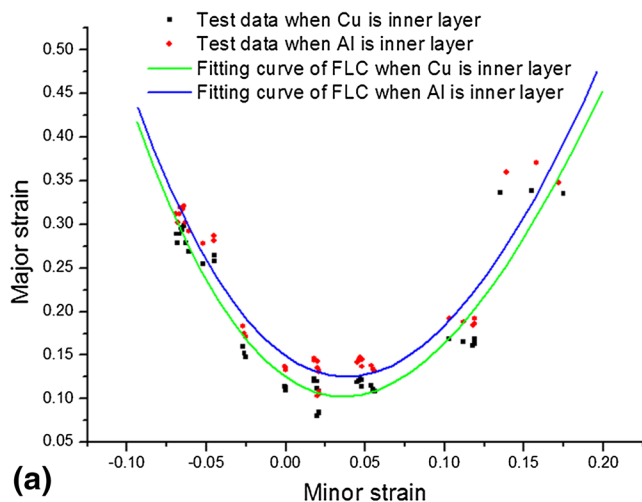


Fig. 9 FLC comparison of DIC method, grid method (XJTUSM), and NADDRG formula. (Color online only)



into contact with the inner Cu layer first, then it remains in the safety zone when the outer Al layer reaches the necking stage. If the punch comes into contact with the inner Al layer first, then it also reaches the failure state when the outer Cu layer arrives. This result suggests that the forming limit of clad metals not only involves the mechanical property but also related to contact status in the forming process.

### 3.3 Failure Analysis of Cu/Al Clad Metals

The cracks in the annealed and non-annealed clad metals are compared in Fig. 6. Although the heat treatment methods are different, Fig. 6 shows that the cracks were off-center for the full-width samples, whereas they were mostly at the center for relatively narrow samples. This result may be due to the different stress states of the samples during the forming process caused by different widths of the samples and the lubrication.

Two typical structures, namely waved interface and flat interface, were observed along the interface of the Cu/Al clad metals as shown in Fig. 11. A powerful impact of up to millions of MPa may have been produced during explosive welding. Such impact could have caused the interface to produce a plastic flow and a high-speed metal jet. The transition area connected to both sides of the metal (but varies with them) was thus generated under the action of the plastic flow and high-speed jet.

Figure 12 shows that the fracture morphologies of the Cu and Al sides are distinctive. The large dimple fracture at the Al side is evident. Thus, the strain rate of Al layer is slow during the forming process. However, neither the dimple fracture nor river pattern could be found at the Cu side. This result may have been obtained because the Cu has a surface-centered cubic structure, and the dissociation face could not be formed as a result of the excellent ductility of Cu. When the Al layer fractures, the Cu layer remains in the safety zone. As such, the strain rates between the Al layer and the Cu layer are inconsonant during the forming process. Figure 12 shows that

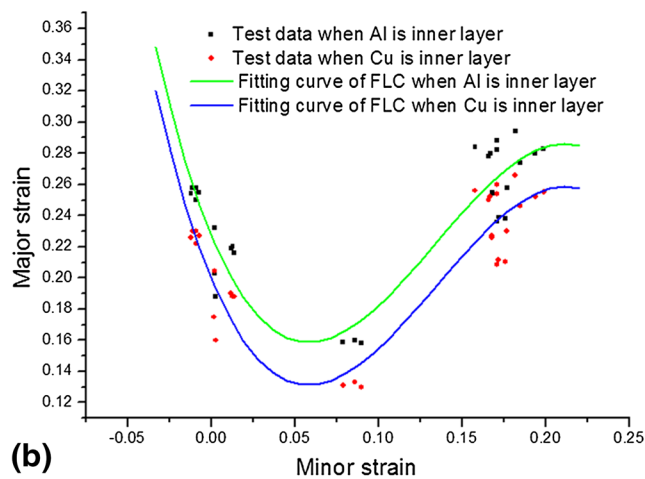


Fig. 10 Forming limit curves of (a) non-annealed and (b) annealed at 280 °C Cu/Al clad metals (Color online only)

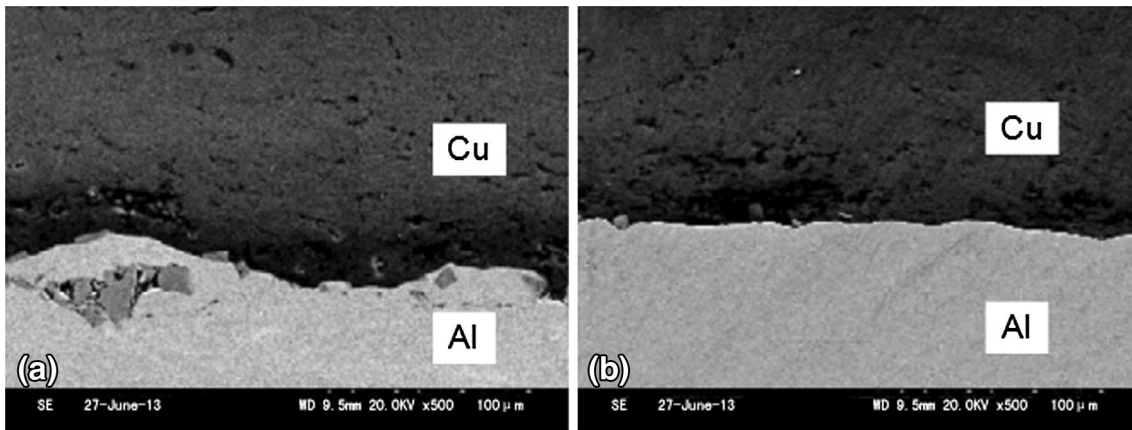


Fig. 11 Interface structure of Cu/Al clad metals: (a) waved interface and (b) flat interface

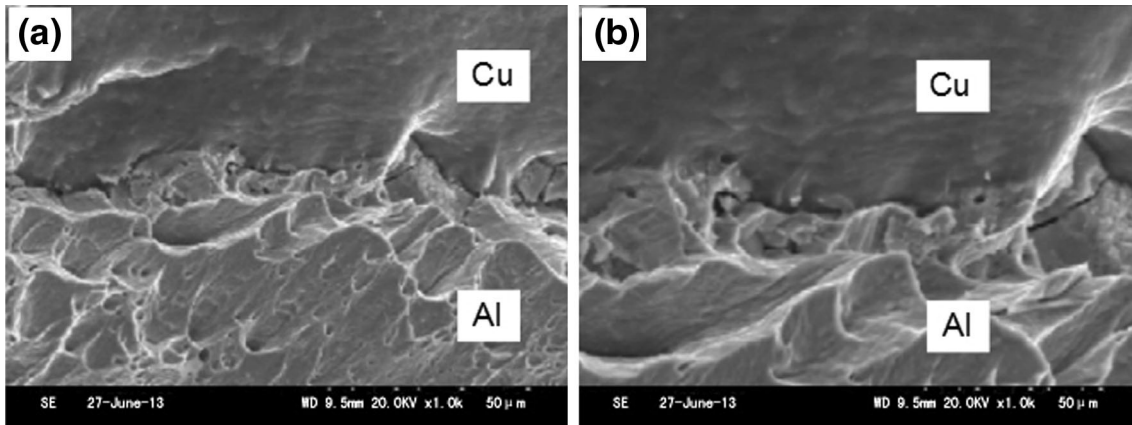


Fig. 12 Fracture structure of Cu/Al clad metals: (a) fracture structure and (b) enlarged drawing of interface fracture

local interfacial failure occurs near the interface between Al layer and Cu layer. However, crack initiation could not be found at both sides of the interface. Thus, the local interfacial failure induces the crack, which subsequently results in fractures. Therefore, the interface fracture is the main failure mode of Cu/Al clad metals during the forming process.

## 4. FEM Simulation

### 4.1 FEM Model

In this section, the fracture prediction of Cu/Al clad metal using finite element simulations will be analyzed and verified with forming limit test using DIC method. The forming limit test was modeled with ABAQUS 6.10, meanwhile ABAQUS/Explicit was employed only to predict fracture location during the forming process of the clad metal sheet. In this case, the entire model of a sample with a width of 30 mm and annealed at 280 °C was constructed, as shown in Fig. 13. The Cu/Al clad metal sheet was considered an equivalent isotropic single layer material. The material properties presented in Table 1 were

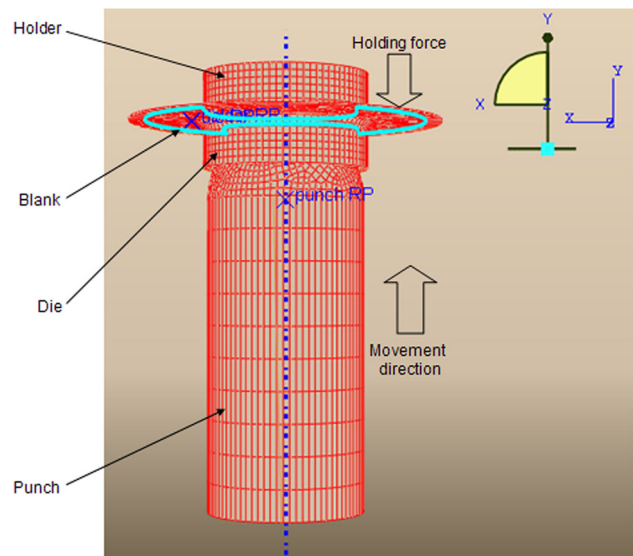
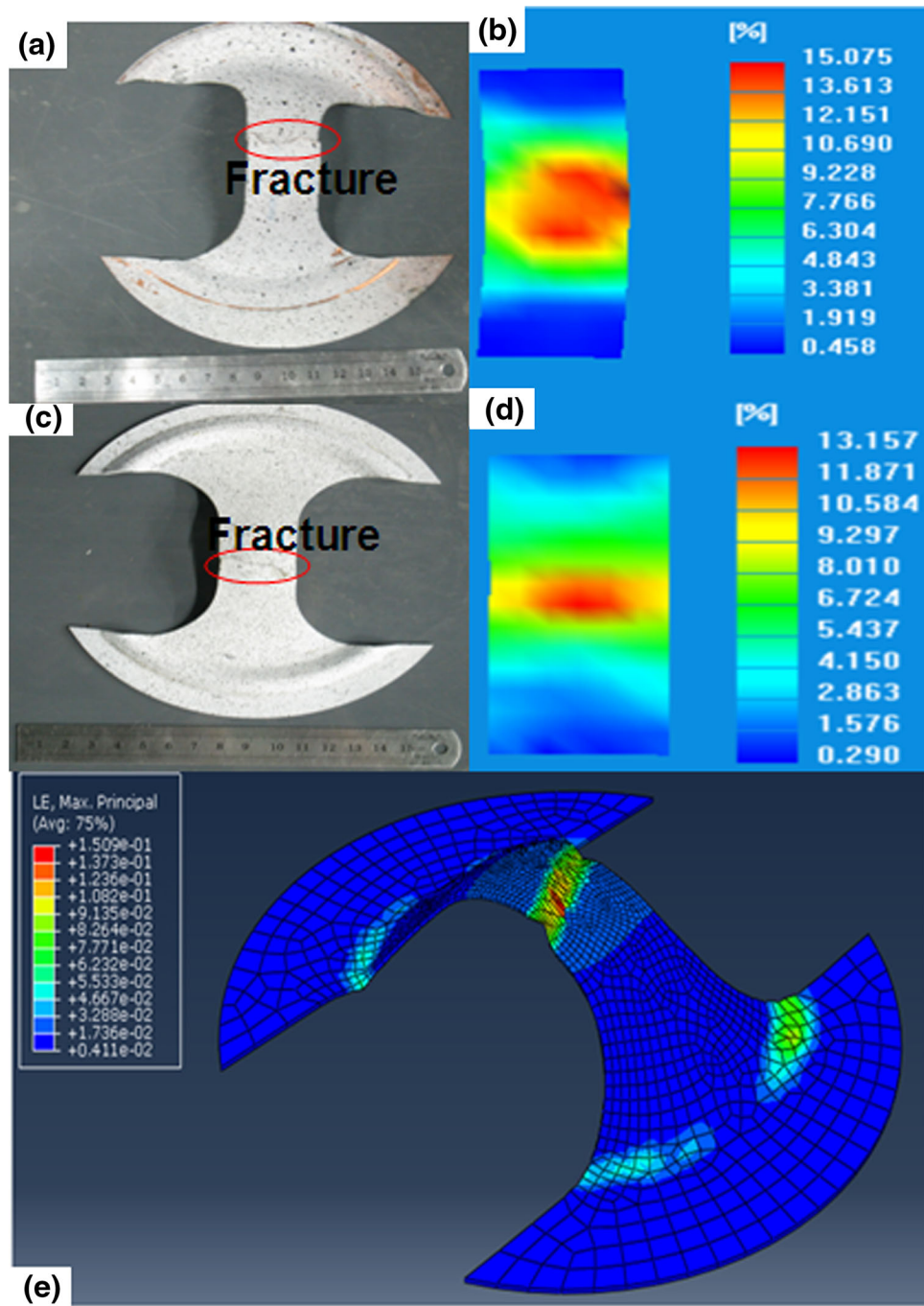


Fig. 13 FEM model of Cu/Al clad metal forming test. (Color online only)





**Fig. 14** FEM simulation of the forming limit test for (a) virtual condition of the sample with Al in the inner layer when fracture occurs and (b) strain contours generated by DIC method with Al in the inner layer and (c) virtual condition of the sample with Cu in the inner layer when fracture occurs and (d) strain contours generated by DIC method with Cu in the inner layer; the fracture site predicted by FEM is shown in (e). (Color online only)

utilized to simulate the actual flow rule of the Cu/Al clad metal sheet. The blank was meshed with quadrilateral solid elements, and the die, punch, and holder were considered discrete rigid bodies.

For the boundary conditions, the punch was specified to move in y direction, and a holding force was applied on the blank through the holder. Three contact pairs (punch-blank, holder-blank, and blank-die) were defined. The Coulomb coefficient of friction was set to 0.1 for all contact surfaces (Ref 3).

#### 4.2 Analysis of the Simulation Result

When the Cu/Al clad metals with Al in the inner layer were tested to complete fracture, failure occurred near the central bulge of the blank; the crack is jagged as shown in Fig. 14(a). Although the fracture location with Cu in the inner layer is also near the central bulge of the sample, the crack line intersects at an angle with the geometric symmetry line of the sample as seen in Fig. 14(c). The strain contours generated by DIC method when Al is in the inner layer or Cu is in the inner layer are

illustrated in Fig. 14(b) and (d), respectively. In both cases, the cracks all are located in the middle of the clad metal sheet caused by uniaxial tensile mode, but the maximum strain distribution is different. The FEM simulation result is shown in Fig. 14(e). The crack is located in the central bulge of the sheet; therefore, the predicted fracture sites of the blank were similar to the experimental results. Moreover, the crack extension direction was very similar to the forming limit test result with Cu in the inner layer. It means that the crack propagation direction is related to contact status in the forming process.

## 5. Conclusions

In this study, a digital image deformation measurement and analysis control system (XJTUDIC 8.0) was used to conduct a contrast test between the DIC method and conventional grid method using a SPCC sheet metal forming limit test. The effects of heat treatment and contact state on Cu/Al clad metal formability were investigated on the basis of the FLC generated by the DIC method. The interfacial and fracture structures were analyzed via SEM. As for the fracture location predictions in Cu/Al clad metal, the finite element model has been verified with forming limit test using DIC method. The following conclusions were drawn from the experimental results:

1. In the FLCs of SPCC, the top region shows the FLCs of SPCC of the NADDRG formula, the middle region shows that of the grid method, and the bottom region shows that of the DIC method. The first two methods overestimate the formability of SPCC. The DIC method is more likely to be reliable.
2. The formability of the annealed Cu/Al clad metals is superior to that of the non-annealed ones. Thus, the effect of heat treatment on material formability is considerable.
3. The FLC of the clad with Al in the inner layer is higher than that of the clad with Cu in the inner layer. Thus, the forming limit depends on the contact status between the punch and the blank in the forming process.
4. The location of macro crack might be closely related to the width of the samples and the lubrication. The differences in terms of fracture microstructure at both Al and Cu sides are considerable. During the forming process, the local interfacial failure occurs first, and then the cracks are induced, which subsequently result in fractures. The interface fracture could be the main failure mode of Cu/Al clad metals.
5. The fracture location of Cu/Al clad metals caused by uniaxial tensile during the forming limit test using DIC method is predicted by FEM accurately. More effort should be focused on improving the finite element model to predict the failure position and other important parameters, such as major and minor strain, dome height, and punch force more accurately during the forming limit test in future studies.

## Acknowledgments

The authors acknowledge the support of the National Natural Science Foundation of China (Grant No. 51421004, 51275378, and 51275389) and the Fundamental Research Funds for the Central Universities. Comments from the anonymous reviewers are also greatly appreciated.

## References

1. M.H. Parsa, I.K. Yamaguchi, and N. Tkakura, Redrawing Analysis of Aluminum Stainless-steel Laminated Sheet Using FEM Simulations and Experiments, *Int. J. Mech. Sci.*, 2001, **43**, p 2331–2347
2. H.W. Liu and C. Guo, Forming limit diagram of Cu-Al clad, *Mater. Sci. Technol.*, 2010, **18**(4), p 560–563 (in Chinese)
3. H.C. Tseng, C.H. Hung, and C.C. Huang, An analysis of the formability of aluminum/copper clad metals with different thicknesses by the finite element method and experiment, *Int. J. Adv. Manuf. Technol.*, 2010, **49**, p 1029–1036
4. M.R. Morovvati, A. Fatemi, and M. Sadighi, Experimental and finite element investigation on wrinkling of circular single layer and two-layer sheet metals in deep drawing process, *Int. J. Adv. Manuf. Technol.*, 2011, **54**, p 113–121
5. P. Vacher, R. Hadder, and R. Arrieux, Determination of the Forming Limit Diagrams Using Image Analysis by the Correlation Method, *CIRP Ann. Manuf. Technol.*, 1999, **48**(1), p 227–230
6. W. Hotz and P. Hänggi, *Determination of Forming Limit Diagrams Using ARAMIS*, Technical report, GOM, Germany, 2000
7. A. Hijazi, N. Yardi, and V. Madhavan, Determination of Forming Limit Curves Using 3D Digital Image Correlation and In Situ Observation. *Proceedings of SAMPE*, 2004, Long Beach, p 16–20
8. G.P. Pires, M.H. Robert, and R. Arrieux, Studies on Drawing of the Aluminium A5052 Alloy in the Thixocast Condition, *J. Mater. Process. Technol.*, 2004, **157–158**, p 596–603
9. G. Palumbo, D. Sorgente, and L. Tricarico, The Design of a Formability Test in Warm Conditions for an AZ31 Magnesium Alloy Avoiding Friction and Strain Rate Effects, *Int. J. Mach. Tools Manuf.*, 2008, **48**, p 1535–1545
10. C.S. Zhang, L. Leotoing, G.Q. Zhao, D. Guines, and E. Ragneau, A Methodology for Evaluating Sheet Formability Combining the Tensile Test with the M-K Model, *Mater. Sci. Eng. A*, 2010, **528**(1), p 480–485
11. G. Palumbo, D. Sorgente, and L. Tricarico, A Numerical and Experimental Investigation of AZ31 Formability at Elevated Temperatures Using a Constant Strain Rate Test, *Mater. Des.*, 2010, **31**, p 1308–1316
12. A. Rohatgi, E.V. Stephens, A. Soulami, R.W. Davies, and M.T. Smith, Experimental Characterization of Sheet Metal Deformation During Electro-Hydraulic Forming, *J. Mater. Process. Technol.*, 2011, **211**(11), p 1824–1833
13. W. Tong, H. Tao, X. Jiang, N. Zhang, M.P. Marya, L.G. Hector, Jr., and X.Q. Gayden, Deformation and Fracture of Miniature Tensile Bars with Resistance Spot Weld Microstructures: An Application of Digital Image Correlation to Dual-Phase Steels, *Metall. Mater. Trans. A*, 2005, **36**, p 2651–2669
14. Z.Z. Tang, J. Liang, Z.Z. Xiao, C. Guo, and H. Hu, Three-Dimensional Digital Image Correlation System for Deformation Measurement in Experimental Mechanics, *Opt. Eng.*, 2010, **49**(10), p 103601
15. B.Q. Shi and J. Liang, Circular Grid Pattern Based Surface Strain Measurement System for Sheet Metal Forming, *Opt. Laser. Eng.*, 2012, **50**, p 1186–1195
16. S.B. Levy, *A Comparison of Empirical Forming Limit Curves for Low Carbon Steel with Theoretical Forming Limit Curves of Ramaekers and Bongaerts*, IDDRGWG3, Ungarn, 13-14 June, 1996